Jordan Journal of Civil Engineering, Volume **15**, No. **3**, **2021**

Investigation of the Torsional Behavior of Circumferential Joints in a Large-diameter Curved Tunnel

Yuchao Zhang [1)]***, Mengxi Zhang*** [1)*] ***and Xiaochun Xiao*** [2)]

[1)] School of Mechanics and Engineering Science, Shanghai University, Shanghai, China.
[2)] Shanghai Tunneling Engineering Co., Ltd., Shanghai, China.
*Corresponding Author. E-Mail: mxzhang@i.shu.edu.cn

ABSTRACT

Unlike a straight tunnel, a curved tunnel is subjected to torque in the out-of-plane direction. However, the effect of torque is seldom considered in the structural design of curved tunnels. This paper investigates the torsional behavior of circumferential joints in a large-diameter curved tunnel by the finite element method (FEM). The parameters used in the three-dimensional model are verified through a prototype test. Graphs of torque *vs*. twist angle for a typical tapered ring lining model are obtained and the torsion stiffness is calculated and compared with results from a parallel ring lining model under different conditions (angle of bolts, strength grade of bolts, residual longitudinal load). The results indicated that the structural behavior of the tapered ring lining cannot be approximated by a parallel ring lining; the torsional stiffness depends on the working conditions. The results of this research may provide guidance for the design of similar tunnels.

KEYWORDS: Tapered ring lining, Curved tunnel, Torsion behavior, Longitudinal deformation.

INTRODUCTION

With the development of urban areas, tunnels are required to have sharp turns in both directions to avoid underground structures; for example, in the newly built Shanghai North Highway Tunneling project. The tunnel is in the northern part of Shanghai, where it relieves traffic congestion. The external diameter of the tunnel is 15 m, which is by far the largest in use and the whole length spans 6.4 km. The longitudinal design of the Shanghai North Highway tunnel poses a great challenge to structural designers, because it features multiple continuous sharp curves (the smallest radius of curvature is 500 m) (Figure 1). The method for designing very long curved tunnels has not been improved yet, because the structural behavior differs for curved and straight tunnels and there are no similar cases for guidance.

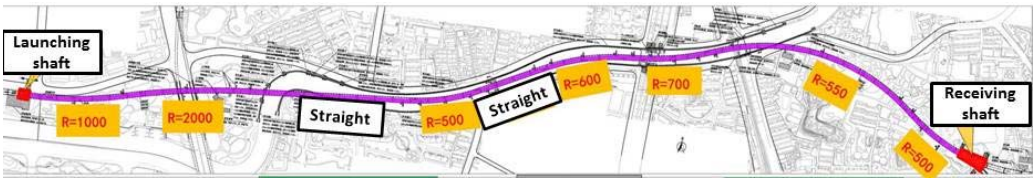

Figure (1): Plan of the newly built Shanghai North Highway Tunnel

As shown in Figure 2, there are basically two approaches for the design of straight tunnels (JSCE, 2007; Koizumi and Guan, 2012; Oh and Moon, 2018; Zhang et al., 2019; Cui and Ma, 2021). The first approach treats the tunnel as a uniform beam resting on an elastic foundation that reduces bending and shearing stiffness, similar to the effect of a joint. This approach is an 'equalized' method, because the total and local deformations of a tunnel are the same. The second

Received on 8/4/2021.
Accepted for Publication on 30/5/2021.

approach simulates the lining of the tunnel as a discrete beam (with no reduction in stiffness), while the circumferential joints are simulated by a series of load-bearing springs that undergo shearing, rotational and axial movement. The value of the stiffness of each spring is calculated before the model is used. Based on the beam-spring model, Do et al. (2014a; 2014b) proposed a three-dimensional shell-spring model, where the effect of longitudinal and circumferential bolts is also simulated by a series of load-spreading springs. However, this method is time-consuming and requires a high-performance computer.

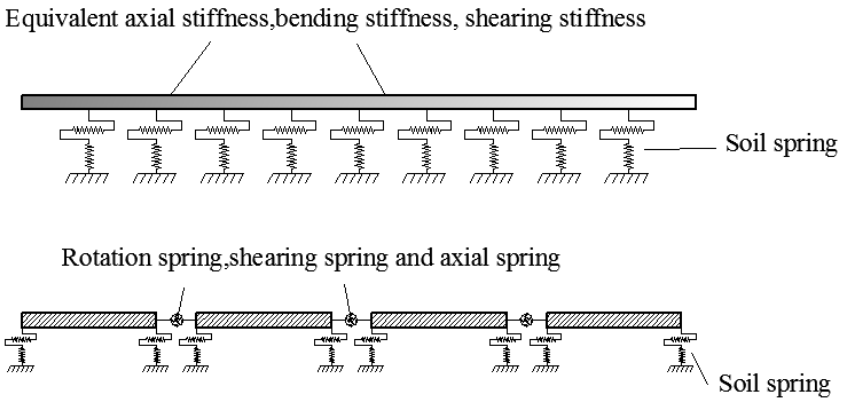

Figure (2): Equivalent stiffness model and beam-spring model

However, as shown in Figure 3, the torque effect should not be neglected if the beam-spring model is selected for the structural design of curved tunnels (Çalım and Akkurt, 2011; Lee and Jeong, 2016). In this figure, *T* represents torque, *M* represents bending moment and *V* is the shearing force. The core mechanism for the torsion behavior of joints is shearing of the bolts and friction at the concrete surface. Many researchers have contributed to the study of the shearing of bolts embedded in different materials (Aziz et al., 2018; Cui et al., 2020; Ghadimi et al., 2016; Hassanieh et al., 2018; Meng et al., 2019; Mirzaghorbanali et al., 2017; Salemi et al., 2015). Salemi et al. (2015) studied the normal and shear resistance of segmental tunnel linings in prototype tests and evaluated the effectiveness of the results by models of beams on elastic foundations. Ghadimi et al. (2016) improved the analytical formula for predicting the shearing behavior of rock bolts embedded in fully grouted rock and then validated the results by FEM testing. Mirzaghorbanali et al. (2017) developed non-contact equipment for investigating the double shearing behavior of cable bolts. Hassanieh et al. (2018) modeled bolt shearing connectors in pockets of cementitious grout and verified them by a prototype test. Based on these studies, the FEM method is selected due to the non-paralleled double shearing faces of tapered ring linings.

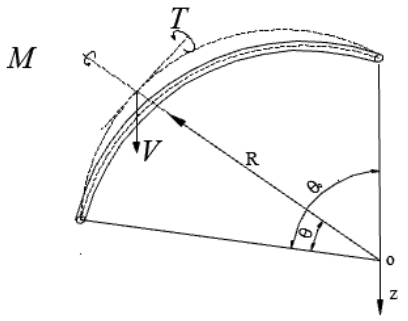

Figure (3): Diagram of internal forces on a curved out-of-plane beam

Very large torque will cause bolts to undergo shear failure, which results in assembly errors in the tunnel. Thus, the main purpose of this paper is to investigate the behavior of circumferential joints under torsion, which may serve as a key element in the beam-spring model.

MATERIALS AND METHODS

Structural Details of the Circumferential Joints

A structural schematic diagram of these two types of linings is shown in Figure 4. The external diameter of the lining is 15 m and its thickness is 0.65 m. A whole ring is divided into ten segments (1 key section, 2 adjoining segments and 7 standard segments). These

segments subtend angles from 19°to 38°. The maximum width of the lining is summarized in Table 1. The degree of taper increases with increasing difference between the maximum and minimum widths. The structural details of the circumferential joints are shown in Figure 5. A typical circumferential joint consists of seal gaskets, two straight bolts and an oblique hole where the bolt is tightened. The angle between the bolt and the interface equals 60°.

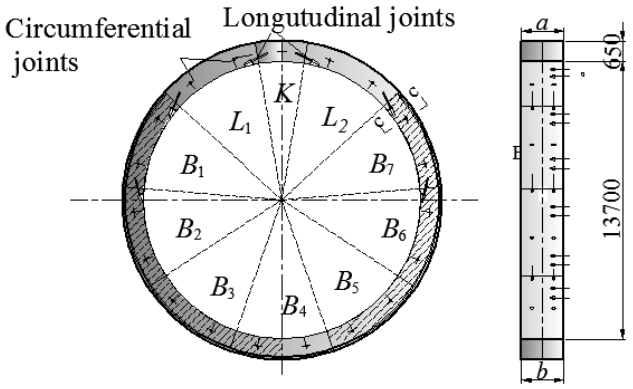

Figure (4): Structural diagram of the segments in a lining ring

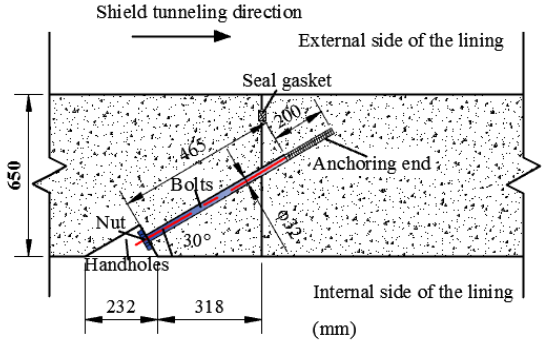

Figure (5): Structural details of circumferential joints

Table 1. Structural parameters of the tapered ring lining

Lining type	a/mm	b/mm	(b-a)/mm	Inclination/x
Tapered ring lining (40 mm)	1980	2020	40	1:750
Tapered ring lining (80 mm)	1960	2040	80	1:375
Parallel ring lining	2000	2000	0	

Finite Element Modeling

The software package ABAQUS 6.14 (Dassault Systemes Simulia Corporation, 2014) is employed to set up the three-dimensional FEM model. The three-dimensional model is shown in Figure 6(a). All the parameters in the FEM model are consistent with the 1:1 prototype model test conducted by the Shanghai Tunnel Design and Research Institute (Li et al., 2011), (Figure 6b). According to the prototype test, the FEM model consists of 1 segment that subtends 19° and two half-segments that subtend 38°.

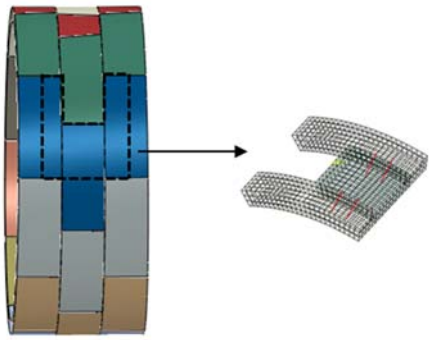

(a) 3D FEM model

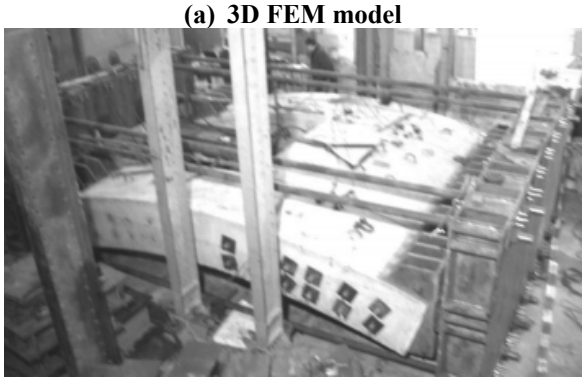

(b) Prototype test model

Figure (6): Finite element model for the lining and bolt based on a prototype model

Parameters Used in the Model

The strength grade of the concrete equals C60 based on the Chinese concrete code (Chinese Ministry of Housing and Urban Development, 2015). A plastic damage constitutive model is employed to simulate and represent the mechanical performance of concrete. The mechanical properties of the concrete are shown in Figure 7. The modulus of elasticity equals 35.5 GPa and Poisson's ratio is 0.18.

High-strength bolts are used in the FEM model; the bolts are made of class 8.8 medium carbon steel that is tempered and quenched. For example, 8.8th grade bolts have tensile strength and yield strength values of 800 MPa and 640 MPa, respectively. An elastoplastic constitutive model is employed to represent the mechanical behavior of the bolts. The modulus of elasticity equals 200 GPa and Poisson's ratio is 0.3. The mechanical properties of the high-strength bolts are listed in Table 2.

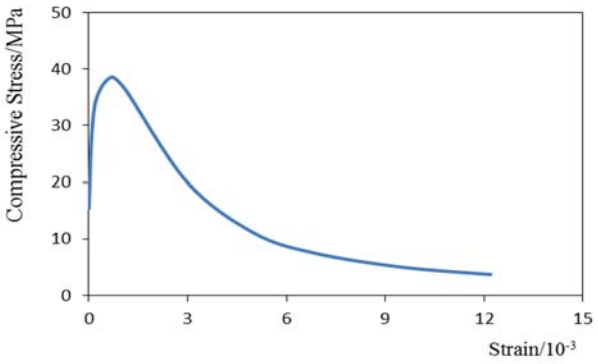

(a) Uniaxial compression

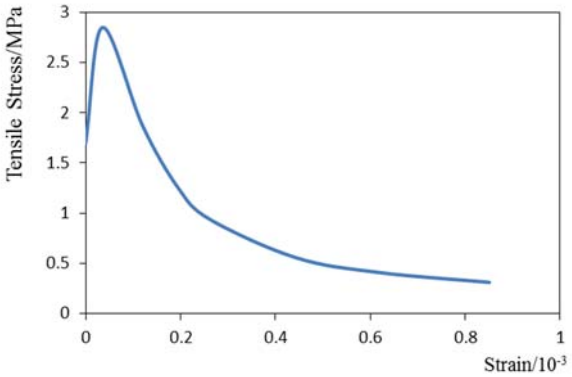

(b) Uniaxial tension

Figure (7): Stress-strain curves of concrete

Table 2. Mechanical properties of bolts

Strength grade of bolt/th grade	Yield strength/MPa	Ultimate strength/MPa
8.8	640	800
9.8	720	900
10.9	900	1000
12.8	1080	1200

Torsion Load and Boundary Conditions

The bolts are embedded in the concrete. The boundary condition of the side concrete is fixed according to the prototype test (Figure 8). The longitudinal load is defined as F_h and shown in Figure 8. It simulates a residual load in the longitudinal direction when a jack force is applied to the tunnel. According to JSCE Standard (JSCE, 2007), the longitudinal load is determined by the buried depth of the tunnel. The maximum value for F_h is 1400 kPa herein. A torque load is applied to the surface of the middle test segment. In the ABAQUS software package, the middle segment is loaded by the displacement method to increase the speed of calculation.

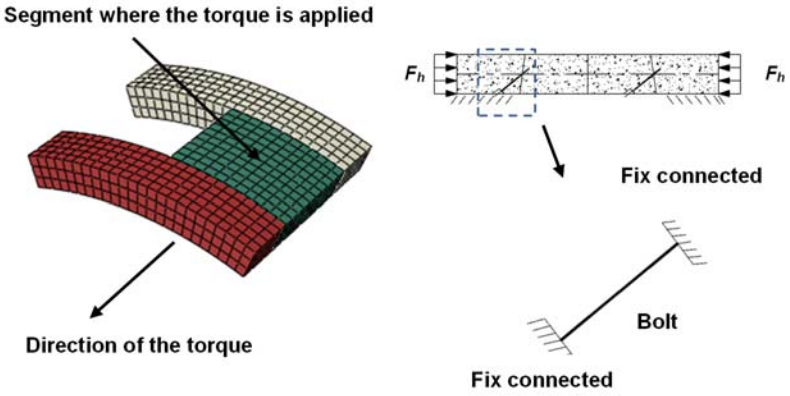

Figure (8): Load and boundary conditions

Verification of the Parameters

According to the prototype test, the strength grade of the bolts is 8.8th. Figure 9 presents the comparison of the measured value and simulated value of the shear force under 2 load conditions. The results for the measured data and simulated values are in good agreement (variation≤ 10%).

RESULTS

Figure 10 presents the stress contour for the concrete. This figure shows that there is a stress concentration in the area where the bolts and the concrete are connected. During the process of twisting, the stresses for the tapered lining models are relatively great compared with those of the parallel ring lining model.

Figure 11 illustrates the curves of the torque and twist angle when the strength grade of the bolt is 8.8th, the angle of the bolts is 60° and the longitudinal load is 1400 kPa. All curves exhibit a two-stage tendency in the process of loading. In the first stage, the torque increases sharply with the increase in twist angle. In the second stage, the torque increases gradually with increasing twist angle. A peak can be found at the end of the first stage. This indicates that the bolts undergo shear failure and the circumferential joints cannot sustain any torque load. Meanwhile, all the curves show almost linear tendencies in these two stages. Torsion stiffness k is defined as the slope of the curve, as shown in Figure 11. The first and second stages of torsion stiffness, k_1 and k_2, will be discussed in the following section. According to the figure, the torsion stiffness is larger for the tapered ring lining than the parallel ring lining model.

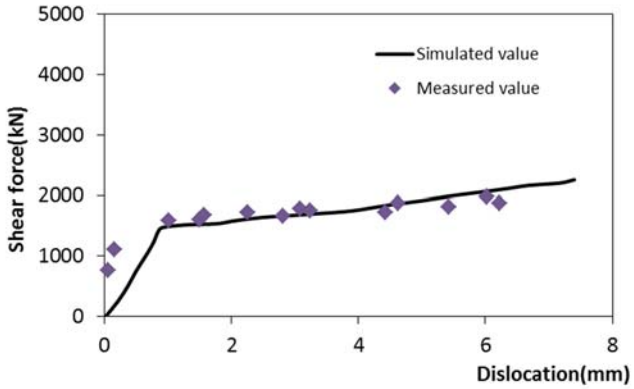

(a) F_h=700kN

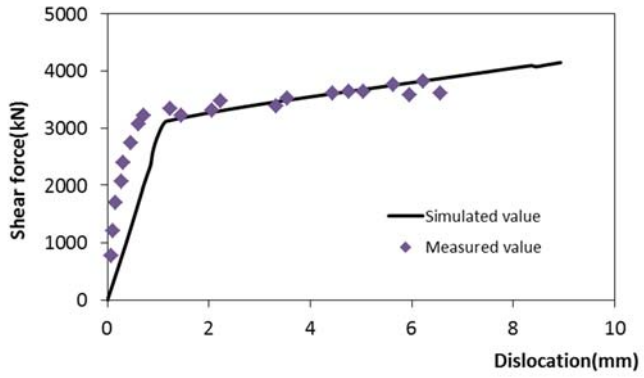

(b) F_h=1400kN

Figure (9): Comparison of the simulated and measured values of the shear force *vs.* dislocation

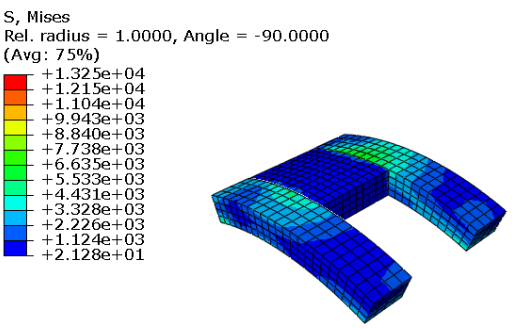

(a) Parallel ring lining

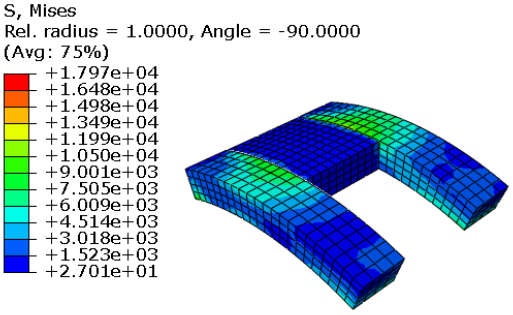

(b) Tapered ring lining (40 mm)

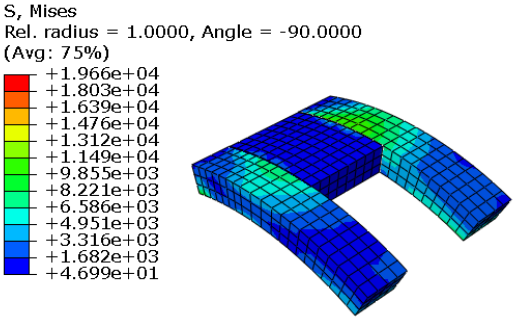

(c) Tapered ring lining (80 mm)

Figure (10): Stress contours of the test segments (kPa)

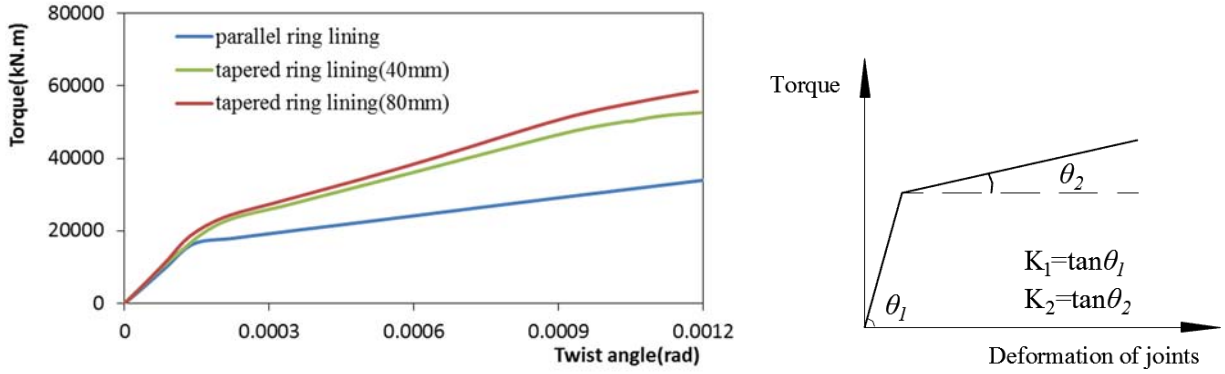

Figure (11): Curves of torque *vs.* twist angle

DISCUSSION

Influence of Bolt Angles

Bolts are generally not installed perpendicular to the joint surface to mitigate differential settlement. The angle of a bolt is defined as the inclination of the bolt axis with reference to the shearing face. Figure 12 illustrates the torsion stiffnesses k_1 and k_2 under different bolt angles. The case occurs when the bolt strength is 8.8th grade and the longitudinal load is 1400 kPa. The first-stage torsion stiffness decreases with increasing angle. However, the second stage torsion stiffness shows the opposite tendency. It can be inferred from the figure that the torsion stiffness increases with increasing taper for the lining model under different bolt angles.

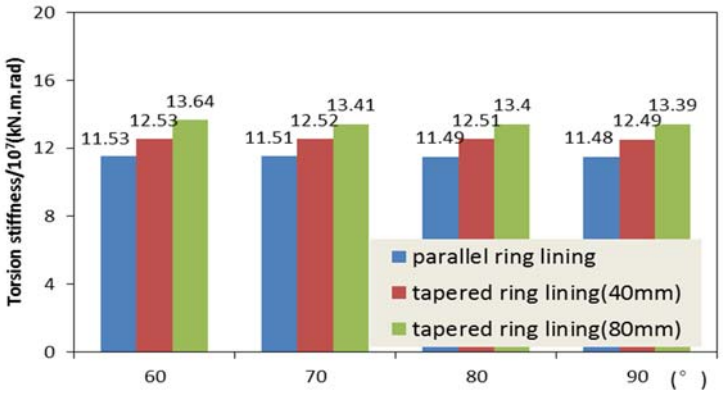

(a)k_1

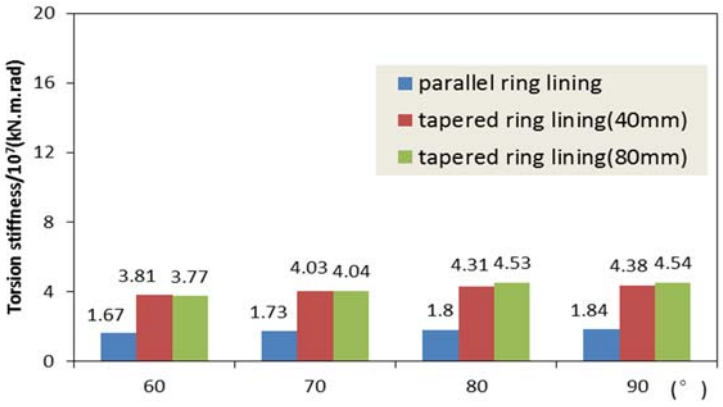

(b)k_2

Figure (12): Torsion stiffness under different bolt angles

Influence of Bolt Strength Grades

Figure 13 illustrates the torsion stiffnesses k_1 and k_2 under different bolt strength grades. The case occurs when the angle is 60° and the longitudinal load is 1400 kPa. The first-stage torsion stiffness does not change, while the second-stage torsion stiffness increases with increasing strength grade. It can be inferred from the figure that the torsion stiffness increases with increasing taper for the lining model under different bolt strength grades.

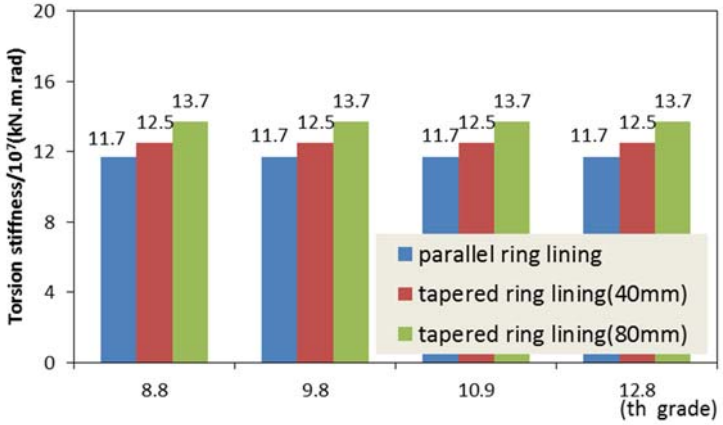

(a)k_1

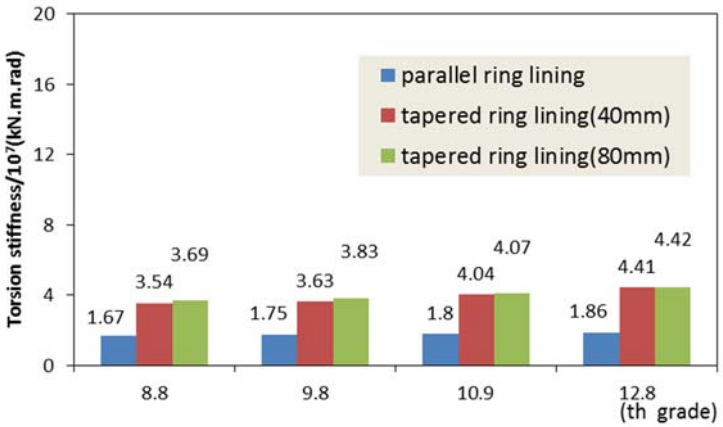

(b)k_2

Figure (13): Torsion stiffness under different bolt strength grades

Influence of Longitudinal Loads

Figure 14 presents torsion stiffnesses k_1 and k_2 under different residual longitudinal loads. The case is when the strength grade is 8.8th grade and the angle is 60°. The first-stage torsion stiffness increases relatively considerably, while the second-stage torsion stiffness decreases with increasing longitudinal load. It can also be concluded that when the degree of taper is greater, then the torsion stiffness value is higher.

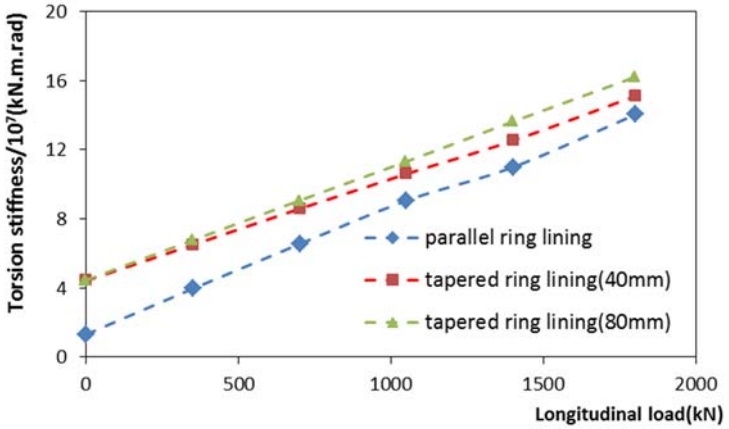

(a)k_1

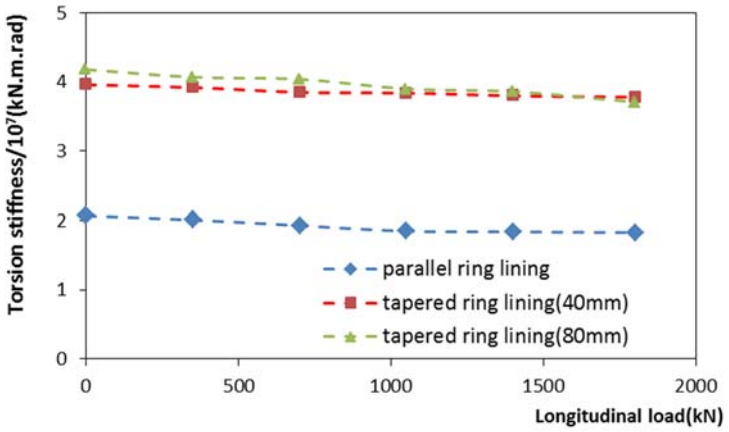

(b)k_2

Figure (14): Torsion stiffness under different longitudinal loads

CONCLUSIONS

This paper presents a finite element analysis of the effects of torque on the structural behavior of circumferential joints with tapered and parallel ring linings. The graphs of load and displacement are obtained from the tests and the torsion stiffness values are derived from the curves. Conclusions are listed as follows:

(a) The graphs of torque *vs*. twist angle display a two-stage trend for these two types of lining.

(b) The torsion stiffness changes with the change in the angle and strength grade of the bolts as well as the residual longitudinal load.

(c) The torsion stiffness values during the two stages for the tapered ring lining are greater than those for a parallel ring lining model.

Thus, if the beam-spring model is selected for the design of curved tunnels, the torsion stiffness value should not be neglected and must be selected with great care.

Funding Statement: The financial assistance from the National Natural Science Foundation of China under Grant No.52078286 and Shanghai Tunnel Engineering Co., Ltd. under Grant No. S2017-SK-2 is herein much acknowledged.

Conflicts of Interest: The authors declare that they have no conflicts of interest to report regarding the present study.

REFERENCES

Aziz, N., Rasekh, H., Mirzaghorbanali, A., Yang, G.Y., Khaleghparast, S., and Nemcik, J. (2018). "An experimental study on the shear performance of fully encapsulated cable bolts in single-shear test". Rock Mech. Rock Eng., 51, 2207-2221.

Çalım, F.F., and Akkurt, F.G. (2011). "Static and free vibration analysis of straight and circular beams on elastic foundation". Mech. Res. Commun., 38 (2), 89-94.

Chinese Ministry of Housing and Urban Development (2015). "Code for construction of concrete structure". China Architecture Press, Beijing (in Chinese).

Cui, G.J., Zhang, C.Q., Chen, J.L., Yang, F.J., Zhou, H., and Lu, J.J. (2020). "Effect of bolt inclination angle on shear behavior of bolted joints under CNL and CNS conditions." J. Cent. South Univ., 27, 937-950.

Cui, G.Y., and Ma, J.F. (2021). "Application of the isolation layer in tunnel crossing the soft and hard rock junction subjected to seismic waves". Jordan Journal of Civil Engineering, 15 (2), 241-252.

Dassault Systemes Simulia Corporation. (2014). "Abaqus 6.14 user's manual". Paris.

Do, N.A., Dias, D., and Oreste, P. (2014). "Three-dimensional numerical simulation of mechanized twin stacked tunnels in soft ground". J. Zhejiang Univ. Sci. A, 15, 896-913.

Do, N.A., Dias, D., Oreste, P., and Djeran-Maigre, I. (2014). "Three-dimensional numerical simulation for mechanized tunnelling in soft ground: The influence of the joint pattern". Acta Geotech., 9, 673-694.

Ghadimi, M., Shariar, K., and Jalalifar, H. (2016). "A new analytical solution for calculation of the displacement and shear stress of fully grouted rock bolts and numerical verifications". Int. J. Min. Sci. Techno., 26 (6), 1073-1079.

Hassanieh, A., Valipour, H., and Bradford, M. (2018). "Bolt shear connectors in grout pockets: Finite element modeling and parametric study". Constr. Build. Mater., 176, 179-192.

JSCE (Japanese Society of Civil Engineering). (2007). "Shield tunneling method: Investigation, design, construction". China Architecture Press, Beijing (in Chinese).

Koizumi, A., and Guan, L.X. (2012). "Segment design of shield tunnel: From leisurely allowable stress design method to limit state design method". China Architecture, Beijing (in Chinese).

Lee, J.K., and Jeong, S.S. (2016). "Flexural and torsional free vibrations of horizontally curved beams on pasternak foundations". App. Math. Model., 40 (3), 2242-2256.

Li, D.M., Chen, Z.J., and Yang, Z.H. (2011). "Test and analysis of shear performance of circumferential joint of segment ring in Shanghai Yangtze river tunnel". Undergr. Eng. Tunn., 1, 15-17 (in Chinese).

Meng, B., Jing, H.W., Yang, S.Q., Cui, T. and Li, B. (2019). "Experimental study on shear behavior of bolted cement mortar blocks under constant normal stiffness". KSCE J. Civ. Eng., 23, 3724-3734.

Mirzaghorbanali, A., Rasekh, H., Aziz, N., Yang, G.Y., Khaleghparast, S., and Nemcikb, J. (2017). "Shear-strength properties of cable bolts using a new double-shear instrument: Experimental study and numerical simulation". Tunn. Undergr. Sp. Tech., 70, 240-253.

Oh, J., and Moon, T. (2018). "Seismic design of a single bored tunnel: Longitudinal deformations and seismic joints". Rock Mech. Rock Eng., 51, 893-910.

Salemi, A., Esmaeili, M., and Sereshki, F. (2015). "Normal and shear resistance of longitudinal contact surfaces of segmental tunnel linings". Int. J. Rock Mech. Min. Sci., 77, 328-338.

Zhang, J., He, C., Geng, P., He, Y., and Wang, W. (2019). "Improved longitudinal seismic deformation method of shield tunnels based on the iteration of the nonlinear stiffness of ring joints". Sustain. Cities Soc., 45, 105-116.